THE UNIVERSITY OF MICHIGAN

College of Engineering

Department of Mechanical Engineering

Cavitation and Multiphase Flow Laboratory

Report No. UMICH 03371-12-T

COMPUTER SIMULATION OF HIGH SPEED COLLISION WITH RAIN DROP

(Combined Spherical-Cylindrical Shape)

by

Yen C. Huang*
F. G. Hammitt**
Wen-Jei Yang***

(Submitted to ASME for Publication)

Financial Support Provided by:

National Science Foundation

Grant No. GK-730

September 1971

* Research Associate (Formerly Doctoral Candidate)
** Professor-In-Charge, Cavitation and Multiphase Flow Labortory
*** Professor

NOMENCLATURE

Symbol	Description
A	Exponent in Tait's equation of state
B	Constant in Tait's equation of state
A_1, A_2, B_1, B_2	Dimensionless coefficients
C	Shock wave velocity
C_o	Sonic velocity
D	Diameter
H_1, H_2	Dimensions of Computation Domain in z- and r-direction, respectively
K	Constant
L	Length
M	Mach number
p	Pressure
p^o	$p/\rho_o C_o V_o$
R	Radius of sphere
R_1	Radius of cylinder
R_m	Location of marker m in r- coordinate
r	Radial coordinate
r^o	r/R
t	Time
t^o	Non-dimensional time, Ct/D
U	Marker velocity component in z-direction
u	Velocity component in z-direction
u_n	Velocity component in normal direction
V	Marker velocity component in r-direction
v	Velocity component in r-direction
v_t	Velocity component in tangential direction
V_o	Impact velocity
x_n	Coordinate in normal direction
x_t	Coordinate in tangential direction
z	Vertical coordinate
z^o	z/L
Z_m	Location of marker m in z-coordinate

α	Stability factor
ρ	Density
Δ	Increment

Subscripts

c	Characteristic parameter
m	Marker index
n	Normal direction
o	Initial value
t	Tangential direction

Superscripts

o	Non-dimensional variable

LIST OF FIGURES

I. INTRODUCTION

In recent years, there is growing concern with erosion from the severe local pressures and pressure changes due to liquid impingement on high speed machinery and aircraft components. However, the earliest attention[1, 2] for liquid impact erosion arose in hydraulic (Pelton) and wet steam turbines. When the steam turbine stages operate in the region of vapro-liquid mixture, after the steam has expanded from the high pressure state, the liquid droplets are impacted by the rotating blades at about the operating speed of the turbine[3, 4, 5]. With the higher velocities in the very large new turbine designs, it is likely that the erosion problem can no longer be met through improved materials.

Likewise, in the late 1940's when the speeds of aircraft exceeded Mach 0.5, rapid erosion was experienced by aircraft flying through rain[6] particularly on propellor blades. The problem has become increasingly severe with the present much higher speed aircraft, and also with helicopter blades. Research has been sponsored in this country[7] and also in many other countries,[8] with attention focusing now on radome, window, and structural materials of fixed-wing aircraft and helicopters, as well as missiles to avoid degraded performance and possible failure. The phenomena are similar to the liquid droplet impact erosion of steam trubines and hydraulic Pelton turbines.

It has been suggested[9, 10, etc.] that the damaging mechanism of cavitation may actually be a liquid jet impingement resulting from the non-symmetrical collapse of a bubble. Cavitation erosion is important for high speed ship propellers and other components as well as many other power plant components such as pumps, etc.[11]. It is also a problem in turbines[12, 13] and pumps[14, 15] of space

power plants using liquid metals as the working fluid, as well as in present sodium-cooled fast breeder reactor power plants and in many other cases involving many different fluids.[11]

Soil erosion caused by raindrop impact, a rather analogous phenomenon, also has received attention[16] in the present tide of interest in ecology.

Liquid droplet impact on a solid surface has been observed for centuries. The first extensive description of this phenomena was that given by Worthington[17] around 1894. Considerable pioneering work since the early 1950's was conducted by Dr. Olive Engel[18] Her work[19] includes a chemical mapping of the radial water flow on the impact plane, the use of high-speed motion-picture photography to record the motion of the impacting water drop, and the use of Schlieren photography to study details in the radial flow. Bowden and Brunton[20] reported on fundamental studies of liquid jet impact at supersonic speed. Recently, Fyall[21] used a turbine-driven Barr and Stroud CP5 rotating mirror camera (2×10^5 - 8×10^6 pps) to record photographically the collision process of a moving target with a single stationary water drop in order to study the basic mechanisms of rain erosion. A rather similar camera is being used in the author's laboratory to study the impact of moving water droplets with stationary surfaces. The above are merely typical citations from a very numerous and growing literature in this field.

Photographic studies[19, 20, 21] have shown that the maximum lateral velocity typically considerably exceeds the impact velocity. The resulting sheet of liquid spreads radially around the periphery of the contact zone, while the remaining portion of the drop is relatively undeformed. This suggests that compressibility effects are important in the liquid-solid impact phenomena.

In the initial stages of the impact, the sudden deceleration of the liquid will establish a large pressure gradient. The spatial

gradients of velocities are negligible compared with the large magnitude of local acceleration.

For the one-dimensional case, during the early phases of impact, the integration of the appropriate equation of motion

$$\rho \frac{\delta v}{\delta t} = - \frac{\delta p}{\delta z} \tag{1-1}$$

yields the well-known "water hammer pressure"

$$p = \rho_o C V_o \tag{1-2}$$

where ρ_o is the density of the ambient liquid, V_o is the impact velocity, and C is the shock wave velocity with respect to the undisturbed liquid. For low impact velocity, C can be reasonably approximated by the acoustic velocity C_o. However, for high impact velocity, the compressibility effect must be taken into account. This requires the equation of state.

Tait[22] in 1888 proposed the following equation of state for water:

$$\frac{p + B}{p_o + B} = \left(\frac{\rho}{\rho_o}\right)^A \tag{1-3}$$

where B and A are two empirical functions of temperature. A = 7.15 and B = 3047 bars at 20°C were given by Cole[23]. Li[24] concluded Tait's equation represents relationship of water properties very well by exhaustive examination of published experimental data. The combination of Equations (1-2) and (1-3) with the equation of continuity yields an implicit function for the shock wave velocity[25] as

$$C^2 = \frac{p_o + B}{\rho_o} \frac{1 - \left(1 - \frac{V_o}{C}\right)^A}{\frac{V_o}{C}\left(1 - \frac{V_o}{C}\right)^A} \tag{1-4}$$

Heymann[26] proposed a linear relationship for the shock wave velocity as an explicit function of impact velocity only

$$C = C_o(1 + 2V_o) \tag{1-5}$$

where C_o is the sonic velocity in the undisturbed liquid. The above expression is in good agreement with measured shock wave velocity data for water from various sources[27, 28, 29, 30, 31]. It is recommended for use only up to $V_o/C_o = 1.2$. A better approximation in quardratic form was derived in ref. 31.

$$\frac{C}{C_o} = 1 + 2\frac{V_o}{C_o} - 0.1\left(\frac{V_o}{C_o}\right)^2 \qquad (1\text{-}6)$$

The equation (1 -6) is applicable up to $\frac{V_o}{C_o} = 3$. Within this range, predictions for C from Equ (1-4) and (1-6) agree to within about 2%.

Savic and Boult[32] presented a mathematical analysis of the low speed impact and spreading of a spherical liquid drop on a rigid surface but did not take compressibility into account.

Engel[19] performed an approximate analysis of spherical droplet liquid-solid impact and modified the water hammer equation as follows, for the plane rigid surface,

$$p = \frac{\gamma}{2} \rho_o C_o V_o \qquad (1\text{-}7)$$

where γ is a coefficient giving the fraction of impact velocity. It was reported that γ approaches unity for high impact velocities.

Heymann[33] presented new quantitative results for the maximum impact pressure generated which is in some cases the order of 3 times the simple water hammer pressure. His analysis assumes that at the first instant of contact, the pressures have already built up to $\rho_o C V_o$. The analysis[34] shows that this assumption may not be valid.

The bulk of prior research on high speed collision with rain drop has been limited to photographic studies, experimental tests and relatively simple analyses. No solution of a two dimensional pressure distribution has yet been made, to the author's knowledge, prior to the present study. The usage of high speed computer technique has made it feasible to solve this complex problem. The main objective of this study is to simulate high speed collision with rain drops by computer and solve for the flow patterns, impact pressure and velocity distribution developed in the rain drop as a function of time.

II. Analysis

To solve the high speed collision of a rain drop on a target, it is desirable to simulate as close by as possible the physical phenomena of the impact process so that the simulation result will be close to the actual response. Depending upon the material, the solid target material may respond to the impact like a rigid body with negligible deformation, an elastic plate, a plastic plate or even as a fluid. The problem treated in its most general aspects requires a detailed investigation of the manner in which the material would behave rheologically under an impact. Some compromise must be made between the complexity of the physical problem and the practical difficulties involved in simulating the model selected. For the present study, the target surface has been assumed to be rigid. The model is significant in representing a limiting case of great theoretical importance, and is a close representation of many actual practical cases.

The air surrounding the rain drop may or may not be influential, and the pressure variation within the air in the vicinity of the liquid-air interface may or may not significantly affect the deformation of the liquid-air interface. However, for the present study, constant atmosphere pressure will be assigned to the surrounding air. Actually, the appearance of shock-waves in the air induced by the target velocity may be of extreme importance in some cases by causing the drop to disintegrate before impact.

Since we are dealing with high speed impact, the effect of compressibility of the liquid must be taken into account in any valid and realistic analysis. However, it is reasonable to neglect the effects of body force and viscosity as compared with pressure and inertia. Similarly, the surfact tension, which is involved in the boundary condition, can also be neglected.

Under these assumptions, the high speed collision process of a rain drop on a flat rigid surface can be described as in the following.

The equations of continutiy and momentum for the liquid drop become:

$$\frac{\partial \rho}{\partial t} + \frac{\partial (\rho u)}{\partial z} + \frac{1}{r} \frac{\partial (r\rho v)}{\partial r} = 0 \qquad (2\text{-}1)$$

$$\frac{\partial (\rho u)}{\partial t} + \frac{\partial (\rho u^2)}{\partial z} + \frac{1}{r} \frac{\partial (r\rho vu)}{\partial r} = -\frac{\partial p}{\partial z} \qquad (2\text{-}2)$$

$$\frac{\partial (\rho v)}{\partial t} + \frac{\partial (\rho vu)}{\partial z} + \frac{1}{r} \frac{o (r\rho v^2)}{\partial r} = - \frac{\partial p}{\partial r} \qquad (2\text{-}3)$$

where u and v are the axial and radial velocity components for the cylindrical coordinates z and r respectively. t is the time variable, and ρ and p are the liquid density and pressure.

Since there are three equations but four unknowns, an additional equation is required to solve the problem, i.e., the equation of state for water in which the density and pressure are coupled.

$$\frac{p + B}{p_o + B} = \left(\frac{\rho}{\rho_o}\right)^A \qquad (2\text{-}4)$$

Since the liquid boundary is free to deform, it is required to keep track of its location. The marker particles imbedded in the boundary follow the equation of motion for a free body and the kinematic relations used in the Lagrangian calculation.

$$\frac{d (mU)}{dt} = F_z \qquad (2\text{-}5)$$

$$\frac{d (mV)}{dt} = F_r \qquad (2\text{-}6)$$

$$U = \frac{dZ_m}{dt} \qquad (2\text{-}7)$$

$$V = \frac{dR_m}{dt} \qquad (2\text{-}8)$$

where mU and mV are the mommentums of a marker particle subject to external forces F_z and F_r in the z- and r- direction respectively. Z_m and R_m describe the location of a marker particle.

The above governing equations, after divided respectively by the characteristic parameters of the problem ρ_c, u_c, v_c, p_c, t_c, z_c, r_c, can be expressed in dimensionless forms:

$$\frac{\partial \rho}{\partial t} + A_1 \frac{\partial(\rho u)}{\partial z} + A_2 \frac{1}{r} \frac{\partial(r\rho v)}{\partial r} = 0 \qquad (2\text{-}9)$$

$$\frac{\partial(\rho u)}{\partial t} + A_1 \frac{\partial(\rho u^2)}{\partial z} + A_2 \frac{1}{r} \frac{\partial(r\rho vu)}{\partial r} = -B_1 \frac{\partial p}{\partial z} \qquad (2\text{-}10)$$

$$\frac{\partial(\rho v)}{\partial t} + A_1 \frac{\partial(\rho uv)}{\partial z} + A_2 \frac{1}{r} \frac{\partial(r\rho v^2)}{\partial r} = -B_2 \frac{\partial p}{\partial r} \qquad (2\text{-}11)$$

$$\frac{p+B}{p_o + B} = \left(\frac{\rho}{\rho_o}\right)^A \qquad (2\text{-}12)$$

$$\frac{d(\rho U)}{dt} = -B_1 \frac{dp}{dz} \qquad (2\text{-}13)$$

$$\frac{d(\rho V)}{dt} = -B_2 \frac{dp}{dr} \qquad (2\text{-}14)$$

$$Z_m = A_1 \int U \, dt \qquad (2\text{-}15)$$

$$R_m = A_2 \int V \, dt \qquad (2\text{-}16)$$

where

$$A_1 = \frac{u_c t_c}{r_c} \qquad A_2 = \frac{u_c t_c}{r_c}$$

$$B_1 = \frac{p_c t_c}{\rho_c u_c z_c} \qquad B_2 = \frac{p_c t_c}{\rho_c u_c r_c} \qquad (2\text{-}17)$$

One may select the characteristic parameters ρ_c, u_c, p_c, t_c, z_c, r_c in such a way that all the coefficients A_1, A_2, B_1, and B_2

considering the nature of the particular problem, the characteristic parameters will be chosen as follows. Characteristic density ρ_c will be the undisturbed density at 1 atm ρ_o. Characteristic velocity u_c will be the impact velocity V_o. Characteristic pressure p_c will be the simple water hammer pressure based on $\rho_o C_o V_o$. z_o and r_c are the cell size dimensions in the z and r directions, respectively. It is convenient in many cases that they be chosen to be equal. There will be a definite relationship between z_c, r_c and the characteristic lengths of the problem, e.g., the length and the diameter of a cylindrical liquid droplet. Characteristic time t_c will be z_c/C, where C is the shock wave velocity defined in the Eqs. (1-4) and (1-6). After such selection of characteristic parameters, the four parameters in the governing equations: A_1, A_2, B_1, B_2 can be reduced to $A_1 = A_2 = M/(1+2M-0.1M^2)$, and $B_1 = B_2 = 1/(1+2M-0.1M^2)$, where $M = V_o/C_o$. These coefficients, which are functions of impact Mach number, characterize the flow problem.

The appropriate initial conditions over the domain of calculation are

$$p = p_o \qquad u = u_o \qquad v = v_o$$

where p_o is the environmental pressure, u_o and v_o are the initial impact velocities in the z- and r- direction respectively. In the case of a normal impact (i.e., perpendicular), $v_o = 0$ of course and $V_o = u_o$. The appropriate boundary conditions are:

i) along the axis of symmetry (z), r = 0, and symmetry requires

$$v = 0, \quad \frac{\partial u}{\partial r} = 0, \quad \frac{\partial p}{\partial r} = 0$$

ii) along the impacted rigid surfaces, z = 0, $\frac{\partial v}{\partial z} = 0$, u=0, $\frac{\partial p}{\partial z} = 0$, for full-slip wall condition.

iii) along the free surface, the incompressible continuity yields

$$p = p_o, \quad \frac{\partial u_n}{\partial x_n} = \frac{\partial v_t}{\partial x_t} = 0$$

where u_n amd v_t are the moving velocity components of the liquid-air interface in the normal x_n and tangential x_t directions of the surface respectively.

iv) along the sides of the finite computational domain, permeable boundary conditions will be imposed, in such a way that the normal spece derivative of the variable vanishes at the boundary,

$$\frac{\partial u}{\partial z} = 0, \quad \frac{\partial v}{\partial z} = 0, \quad \frac{\partial p}{\partial z} = 0 \text{ at } z = H_1$$

$$\frac{\partial u}{\partial r} = 0, \quad \frac{\partial v}{\partial r} = 0, \quad \frac{\partial p}{\partial r} = 0 \text{ at } r = H_2$$

where H_1 and H_2 are sizes of computational domain in the z-and r- direction respectively.

All the above equations are then approximated by finite difference expressions. The problem is solved by advancing the configuration through a set of finite time steps or computational cycles. Each numerical computational cycle consists of the following steps.

1). Marker particles on the fluid boundary are moved to appropriate new positions.

2). The continuity and momentum equations are used to advance the densities and velocities through the time change of one cycle by an explicit technique.

3). The pressures are calculated as a function of densities according to the equation of state, assuming quasi-steady process.

4). Boundary condition values and time counters are adjusted to prepare the next computational cycle.

A detailed discussion of the numerical method, the stability, and the accuracy is given elsewhere (35).

III. RESULTS

In examining the following results, one must keep in mind those boundary conditions at the interfaces of the axisymmetrical liquid droplet. Constant atmospheric pressure at the water-air free surface is imposed. The impact plane, which is perfectly rigid and smooth, has no movement. The properties of water are inviscid, without surface tension, but compressible as well as elastic, The tensile strength of water is taken to be -270 atm., an experiemental result of Briggs[36]. Of course, water will rupture in many circumstances at much smaller tensions, but perhaps not for the very short duration of tension involved. The two constants in the Tait's equation of state for water are A = 7.15 and B = 3008 atm. The shape of an actual rain drop is of course never precisely regular. However, a cylindrical-spherical composite shape (Fig. 1) may resemble an actual rain drop better than other simple shapes, because of the deformation of the rain drop by air resistance before impact. The numerical results for such a cylindrical-spherical composite drop lie in between those for a cylindrical drop[34] and a spherical drop[37].

Fig. 1 shows the deformation history of the simulated rain drop following an impact on a rigid surface at Mach number of 0.2 for free slip boundary condition. The liquid surface on the top side of the rain drop remains relatively undeformed until $t^o = 1$. It is also seen from the figure that the liquid on the top surface decelerates, while the liquid on the shoulder still rush downward with less effect received from the stopping action by the rigid surface. As time progresses, the drop shrinks in height and expands radially near the contact surface.

Fig. 2a through 2e show the isobar distribution within the simulated rain drop at five different instants, $t^o = 0.125, 0.25, 0.5,$

1.5, and 2.5 respectively. The figures illustrate how the pressure waves propagate with time from the contact surface toward the free surface. The isobaric surfaces all end at or near the contact ring (the intersection of contact surface and free surface). Because of the condition of constant atmospheric pressure imposed on the free surface, the compression wave cannot proceed beyond the free surface. Each isobaric surface grows in size, radiating outward from the impact surface. Then, as time elapses, there is more outgoing lateral flow than incoming flow at the center area of the impact surface so that the isobaric surface near the contact area changes from a dome shape to a peanut shell shape (Fig. 2c). Another interesting phenomenon appears on Fig. 2d. A region of negative pressure (where actually a cavity might be expected) was generated by the reflection of a pressure wave from the top surface. At the moment as shown on Fig. 2d, the cavity at the center is shrinking, while the cavity in a form of annular ring is growing. Fig. 2e shows the isobar distribution as the impact parameters begin to approach roughly steady-state conditions. The nondimensional steady-state stagnation pressure in this case is 0.1, i.e., $1/2\,\rho_o V_o^2$ divided by the simple water hammer pressure $\rho_o C_o V_o$, where impact Mach Number $M = V_o/C_o = 0.2$. The peak pressure by this point has shifted on the impact surface from the center of impact to the approximate point where a vertical line, tangent to the initial shape of the rain drop, intersects the rigid surface (Fig. 2e). This shifting of peak pressure on the impact surface is caused by the interaction of radial flow and impacting liquid. The numerical computation was terminated at this instant because the steady state has been reasonably approached and thus most of the important features of the phenomenon have been disclosed.

Better illustration of the pressure distribution on the impact surface and along the axis of symmetry are given in Fig. 3 and 4

respectively. Fig. 3 shows the pressure distribution on the contact surface as it develops with time. The pressures fall sharply at the contact edge because of the boundary condition of constant atmospheric pressure at this location. The figures also depict the peak pressures at various instants as they shift from the center to the contact edge. Fig. 4 shows how the pressure waves propagate from the impact surface along the axis of symmetry. They reach the top surface of the drop, and then relfect as tension waves creating a zone of negative pressure.

Fig. 5 shows the local pressures as a function of time. The maximum pressure was recorded at the stagnation point "b". The pressure at "c" will not increase until contact between liquid and solid occurs at that point. The time rate of pressure increases at locations "b" and "c" are about the same for the initial period of impact. As the radial flow commences the pressure distribution is affected so that the pressure at point "b" starts to decrease while that at "c" continues to increase, reaches to its peak and then falls along with the pressures on the impact surface and finally oscillates about the steady-state stagnation pressure. The pressure at "a" also does not increase until the pressure wave approaches that point, and it will not reach as great a value as that at "b" because of the effect of the free surface. The fact that a "bursting out" of the top surface does not occur supports the fact that the pressure at all locations such as "a" will be lower than that at location "b", increasing so as the distance from the impact surface is increased.

Fig. 6 shows the radial velocity distribution on the impact surface at various instants. The peak radial velocities appear slightly inside the contact edge. The dotted portion of the curves indicate regions where the jetting liquid does not remain in contact with the solid surface. The jetting velocity betins to exceed the impact velocity at $t^{o} \cong 0.25$ and increases to ~ 3 x the impact velocity.

Fig. 7 shows the maximum radial pressure gradient, and its location at any given time on the impact surface. The peak maximum pressure gradient occurs at $t^o \cong 0.5$ (or about 0.. 5 usec for a typical rain drop of 2 mm at 1000 ft/sec impact velocity). The locus of the maximum pressure gradient lies closely within the locus of contact edge. It is conjectured that the erosion may be caused by the shear forces associated with these maxiumu pressure gradients.

Fig. 8 illustrates photographs, by Brunton and Camus,[38] of cavitation within a water drop following an impact on a solid plane, as predicted by these calculations (Fig. 2d).

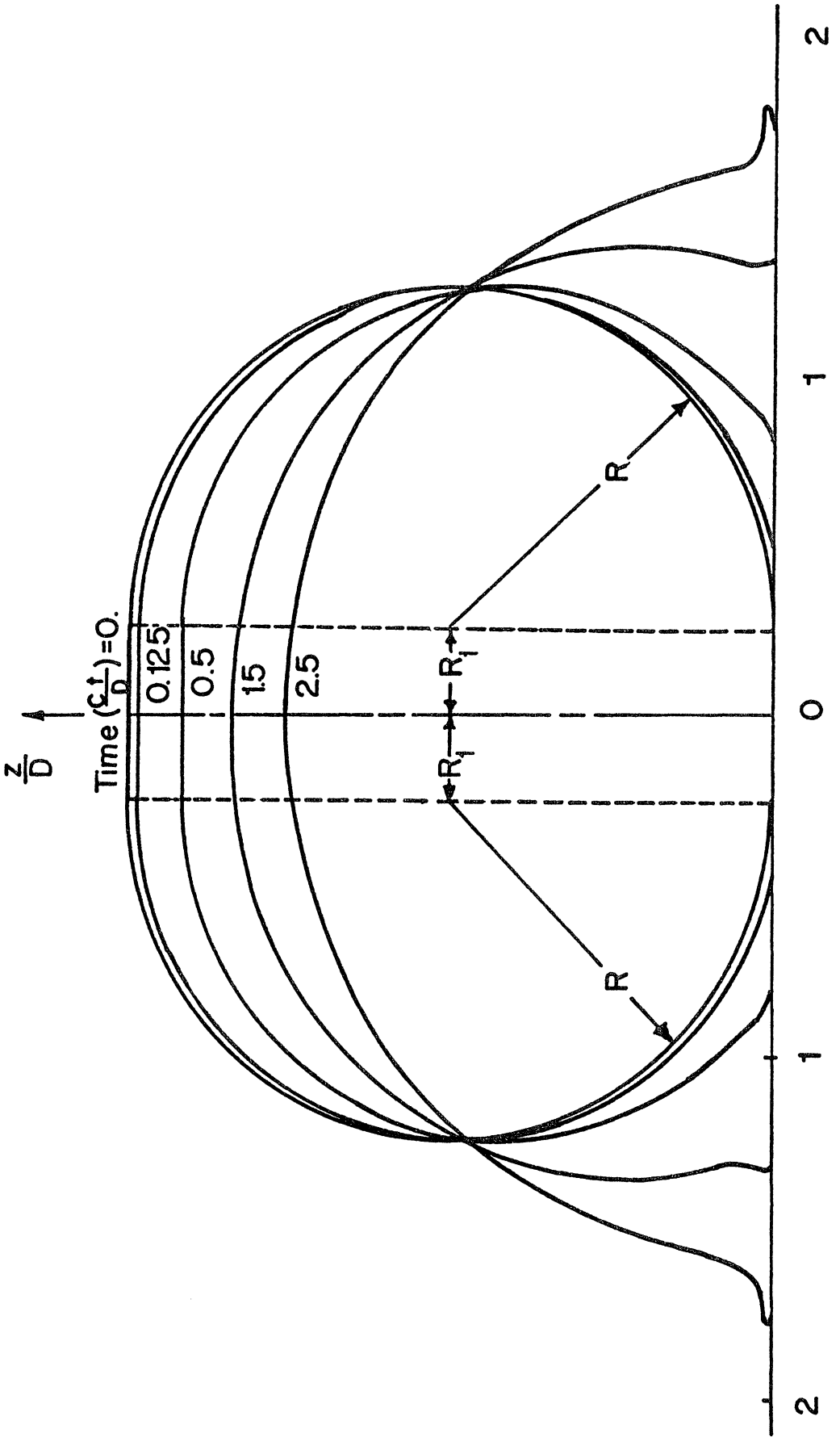

Fig. 1. Shape-Time History of an Initially Cylindrical-Spherical Composite Droplet with R_1/R = 0.25 and L/D = 1, at Mach Number = 0.2, for Free-Slip Boundary Condition.

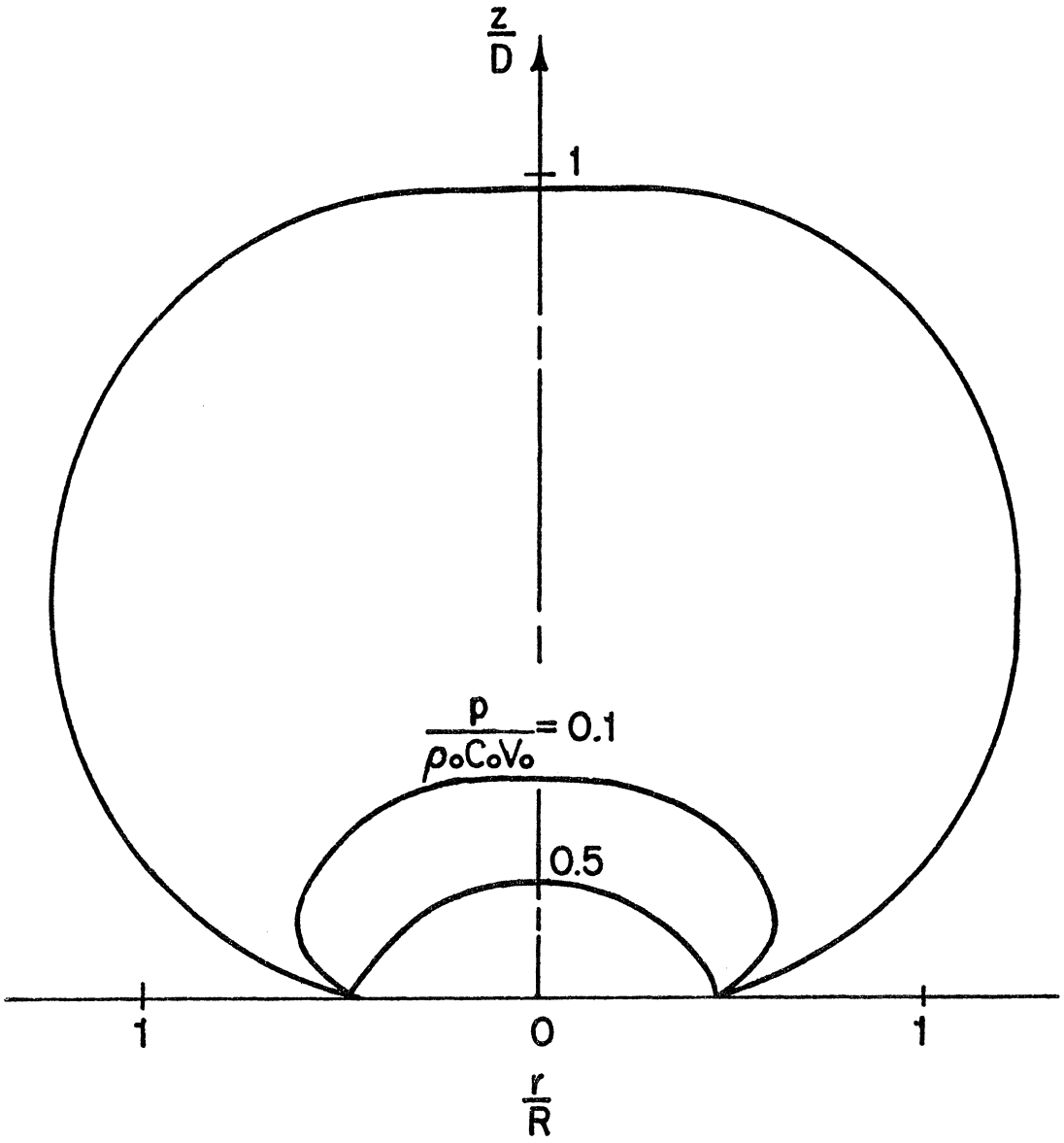

Fig. 2a. Isobar Distribution in an Initially Cylindrical-Spherical Composite Droplet with $R_1/R = 0.25$ and $L/D = 1$, at Time $(Ct/D) = 0.125$, for Impact Mach Number of 0.2 and for Free-Slip Boundary Condition.

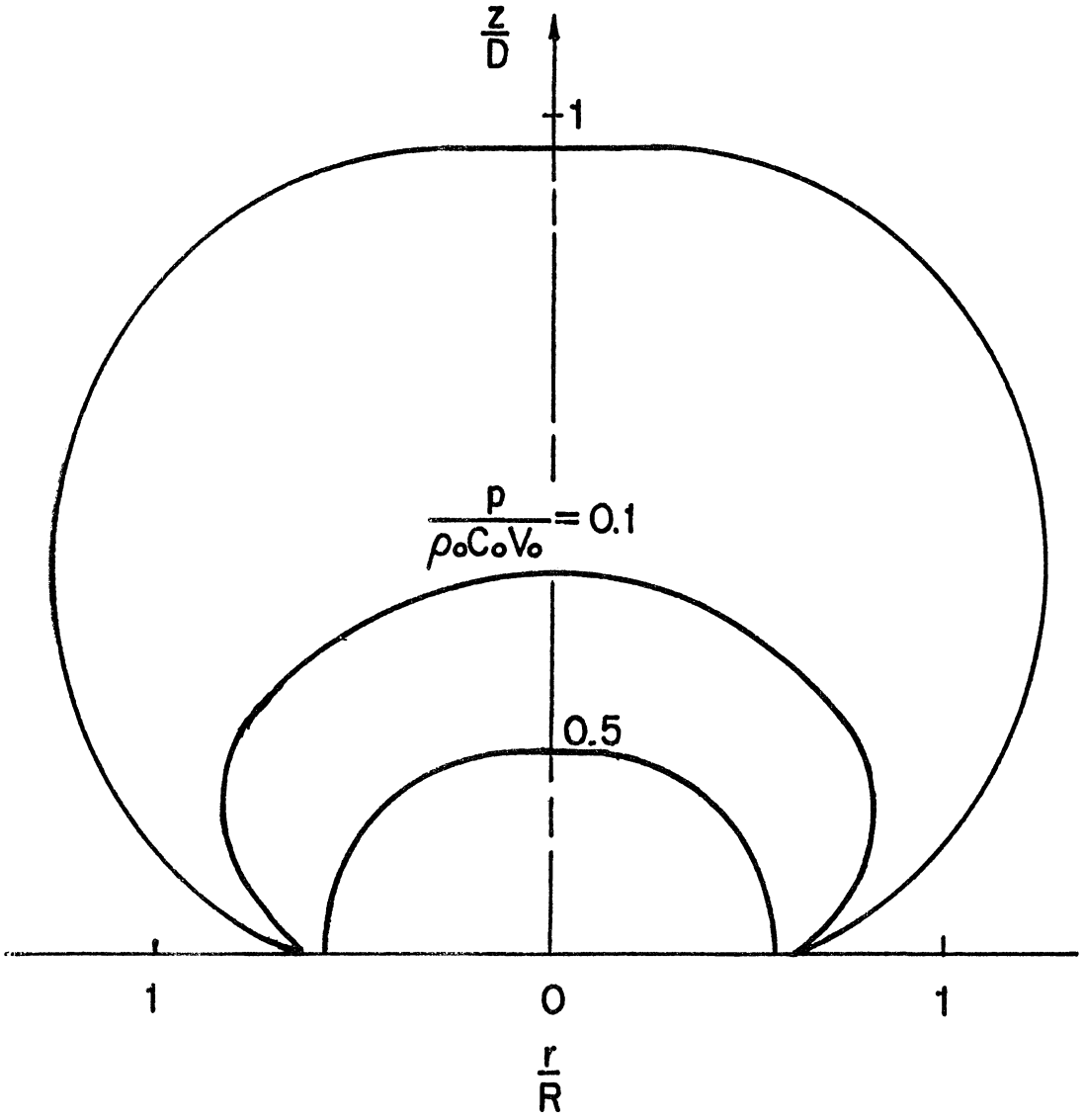

Fig. 2b . Isobar Distribution in an Initially Cylindrical-Spherical Composite Droplet with $R_1/R = 0.25$ and $L/D = 1$, at Time $(Ct/D) = 0.25$, for Impact Mach Number of 0.2 and for Free-Slip Boundary Condition.

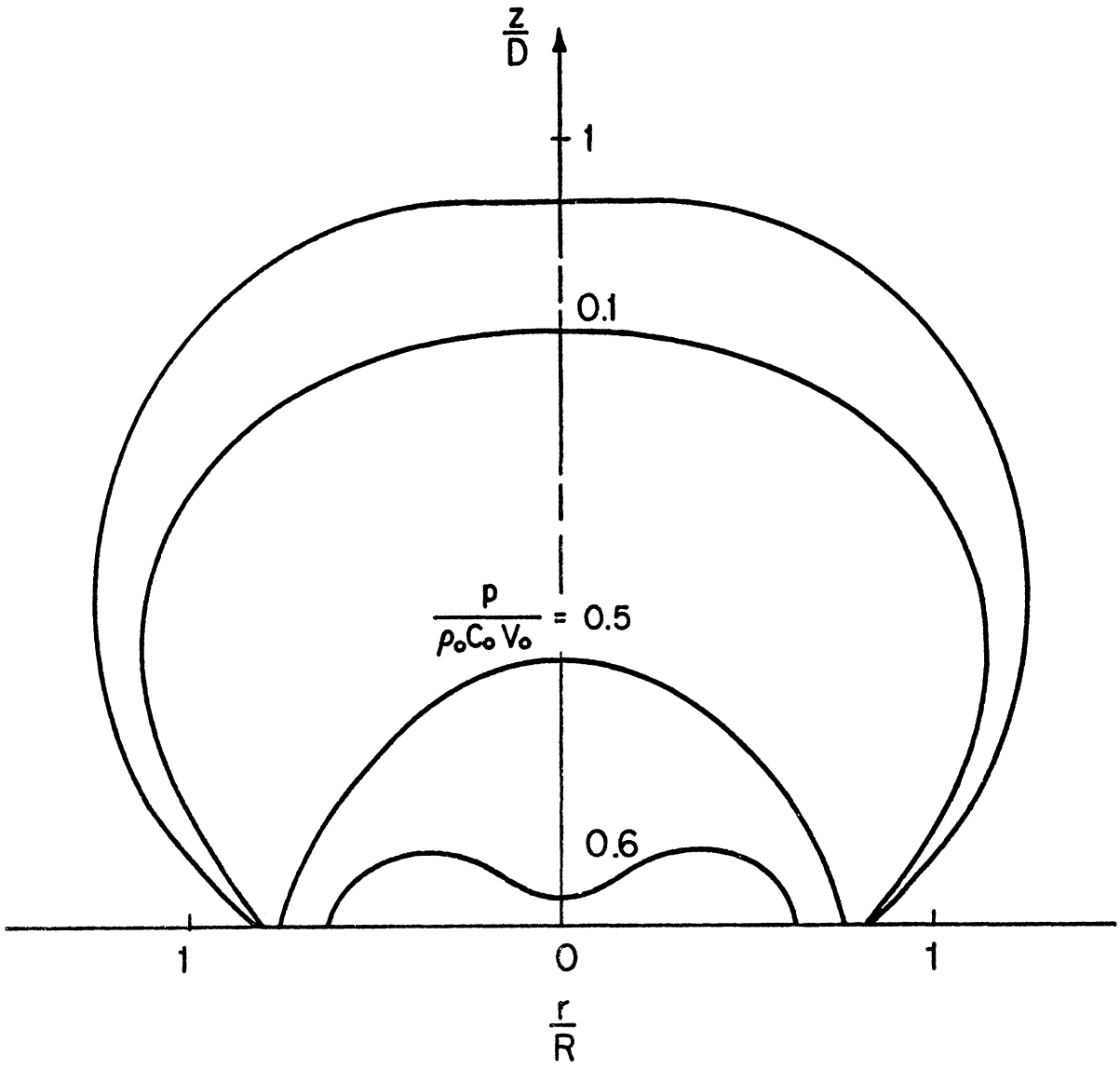

Fig. 2c . Isobar Distribution in an Initially Cylindrical-Spherical Composite Droplet with $R_1/R = 0.25$ and $L/D = 1$, at Time $(Ct/D) = 0.5$, for Impact Mach Number of 0.2 and for Free-Slip Boundary Condition.

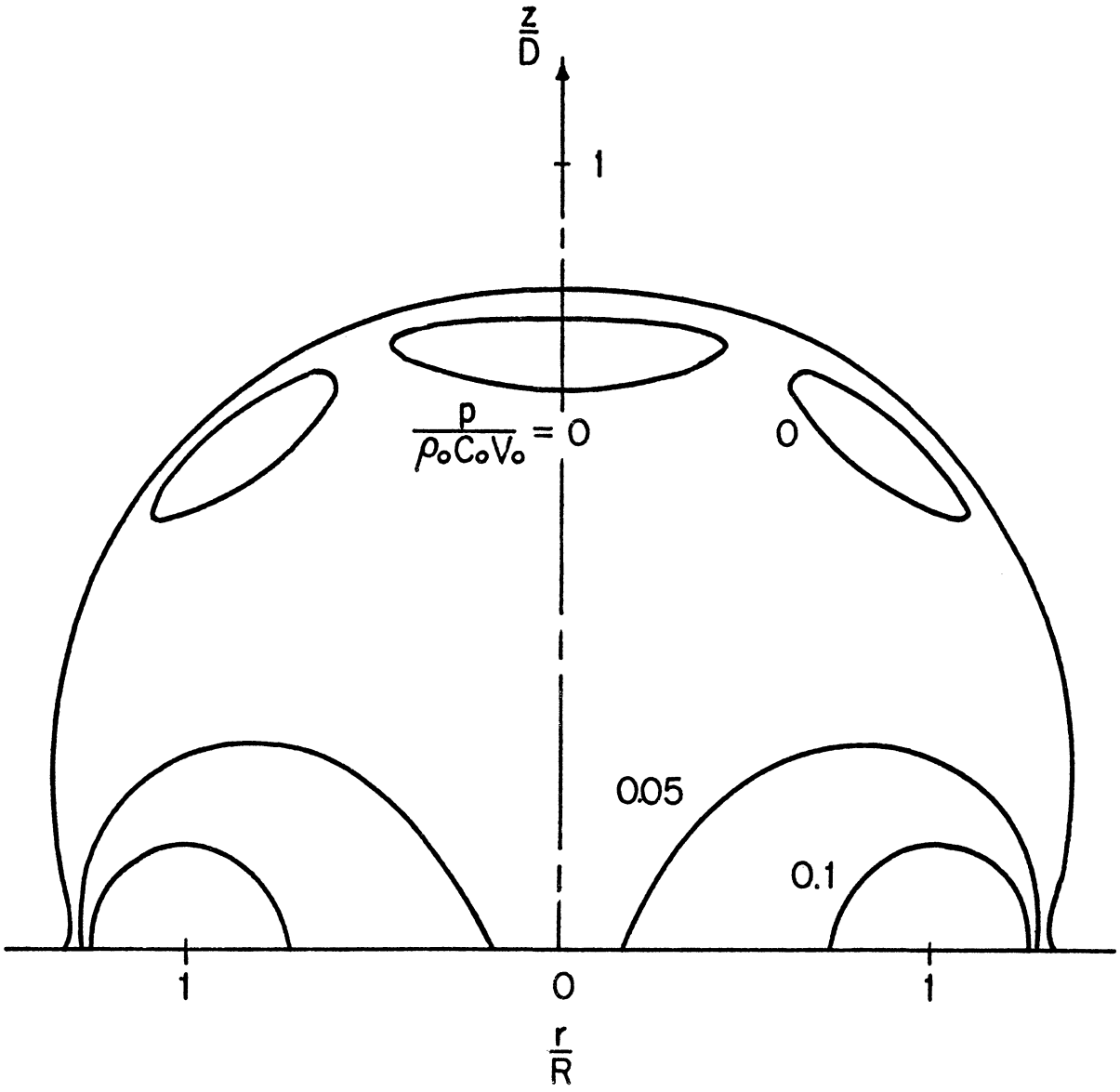

Fig. 2d . Isobar Distribution in an Initially Cylindrical-Spherical Composite Droplet with $R_1/R = 0.25$ and $L/D = 1$, at Time $(Ct/D) = 1.5$ for Impact Mach Number of 0.2 and for Free-Slip Boundary Condition.

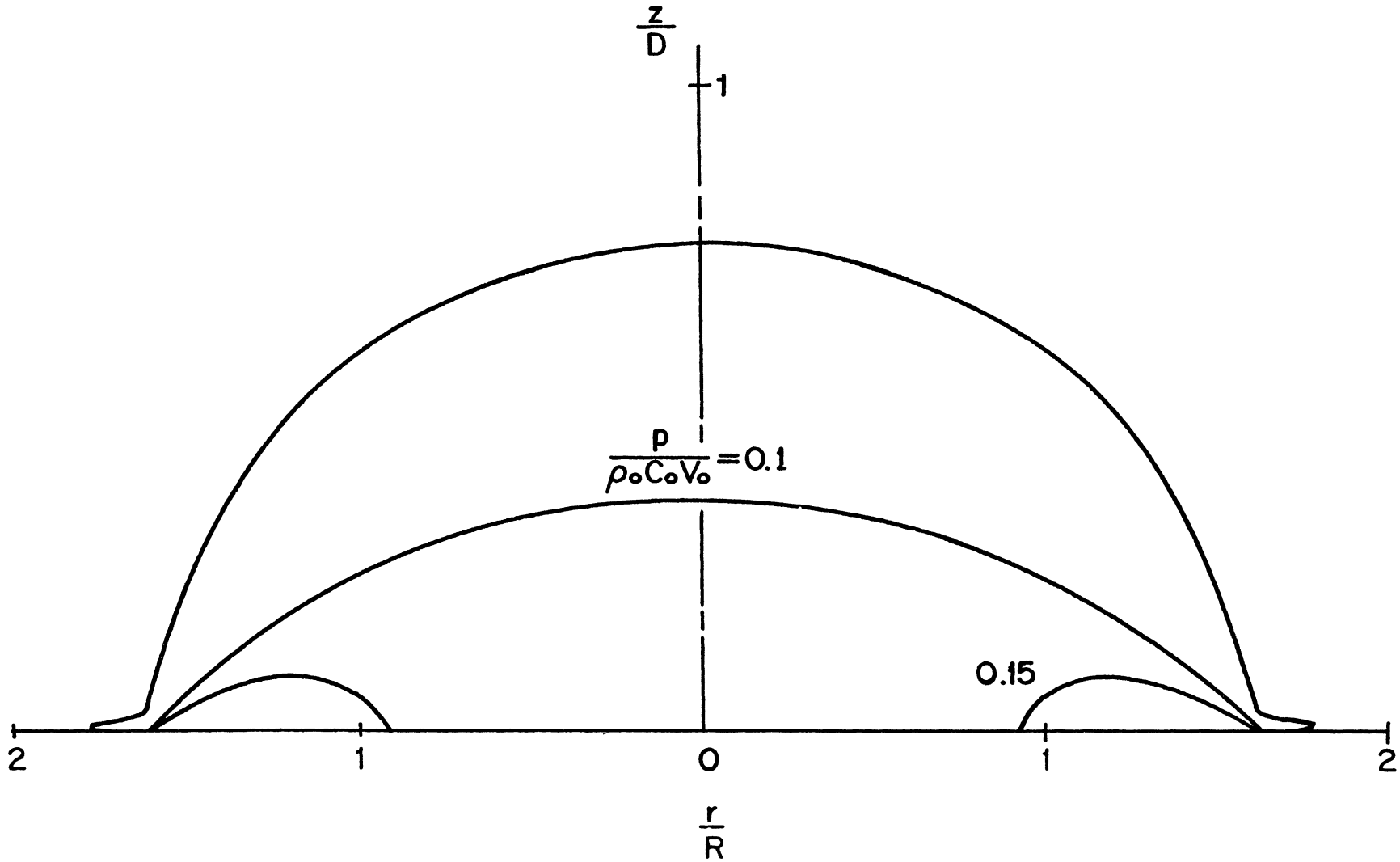

Fig. 2e. Isobar Distribution in an Initially Cylindrical-Spherical Composite Droplet with $R_1/R = 0.25$ and $L/D = 1$, at Time $(Ct/D) = 2.5$, for Impact Mach Number of 0.2 and for Free-Slip Boundary Condition.

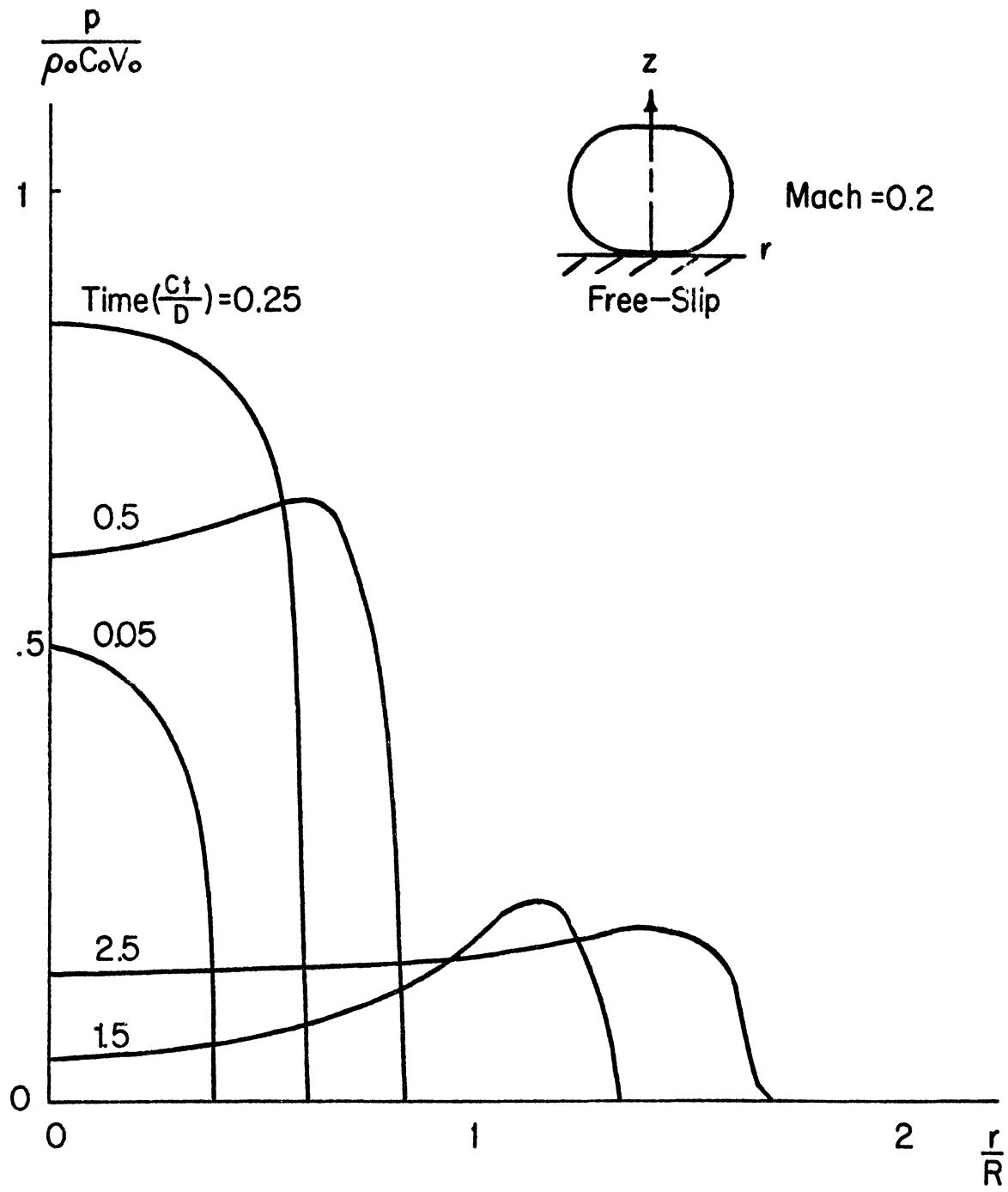

Fig. 3. Pressure-Time History at Liquid-Solid Interface (z = 0) of an Initially Cylindrical-Spherical Composite Droplet with R_1/R = 0.25 and L/D = 1, for Impact Mach Number of 0.2 and for Free-Slip Boundary Condition.

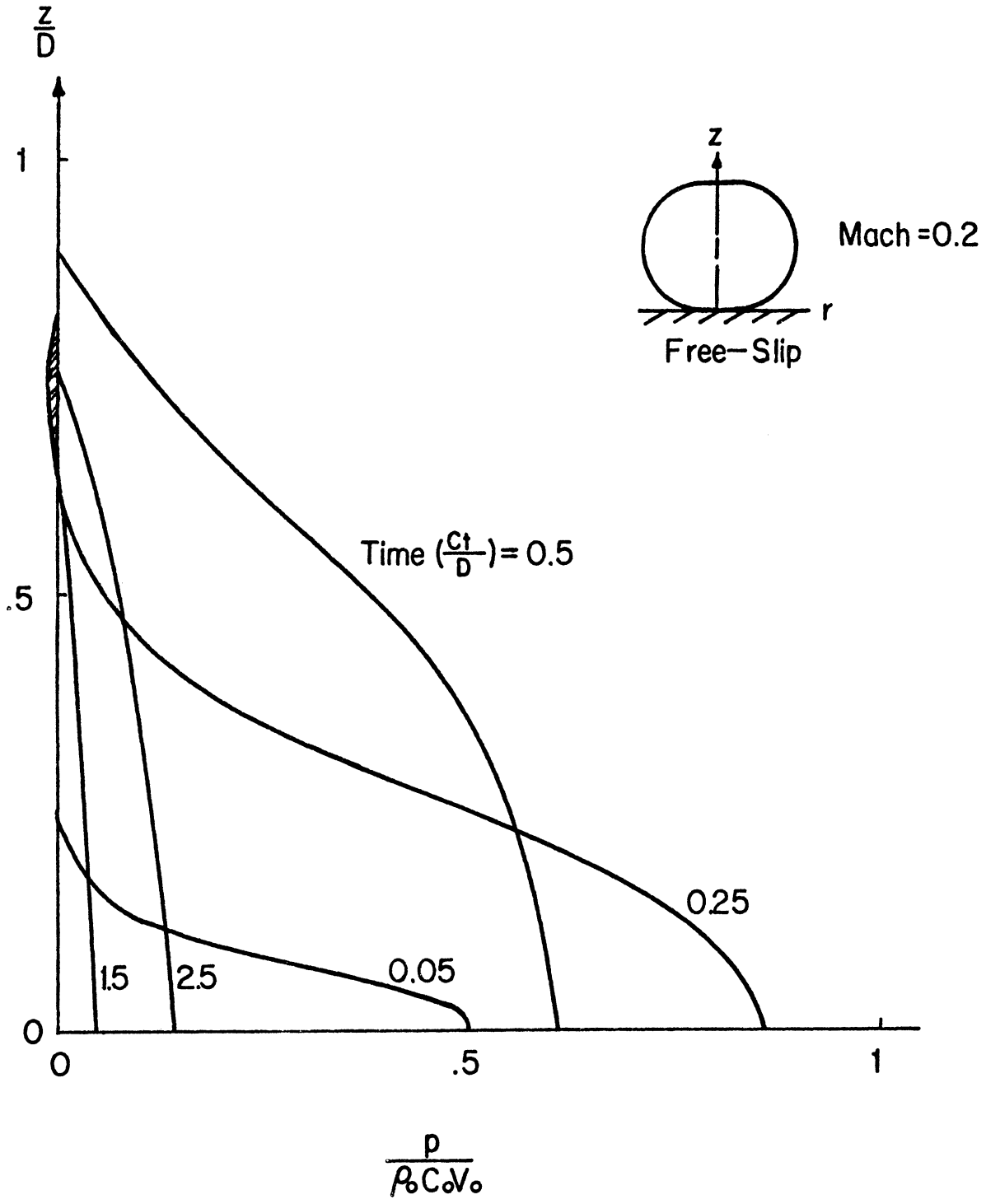

Fig. 4. Pressure-Time History along the Symmetrical Axis (r = 0) of an Initially Cylindrical-Spherical Composite Droplet with $R_1/R = 0.25$ and L/D = 1, for Impact Mach Number of 0.2 and for Free-Slip Boundary Condition.

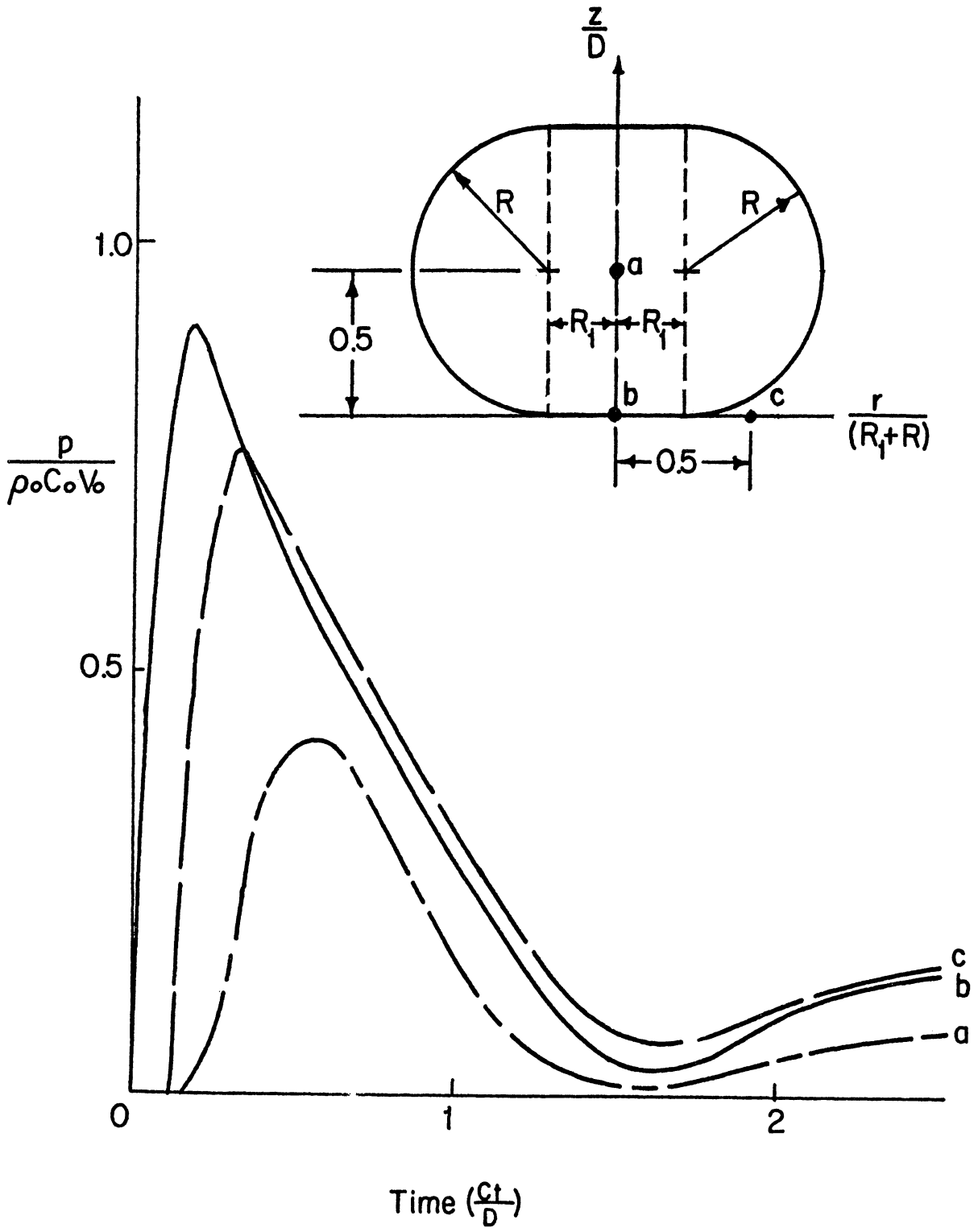

Fig. 5. Local Pressure-Time History at a (r = 0, z = 0.5L), b (r = 0, z = 0), and c (r = 0.75R, z = 0), in an Initially Cylindrical-Spherical Composite Droplet with $R_1/R = 0.25$ and L/D = 1, for Impact Mach Number of 0.2 and for Free-Slip Boundary Condition.

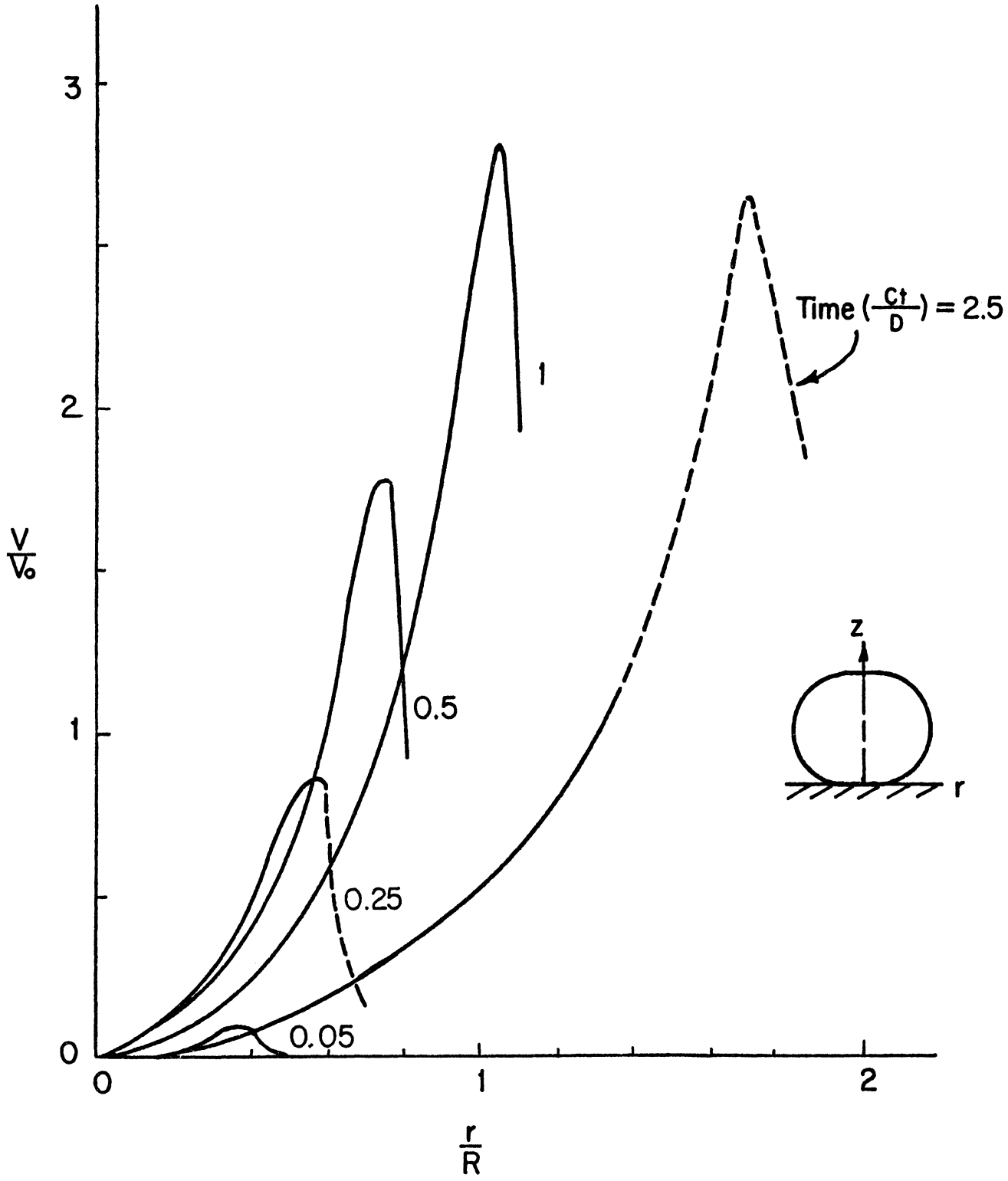

Fig. 6. Radial Velocity-Time History at Liquid-Solid Interface (r = 0) of an Initially Cylindrical-Spherical Composite Droplet with $R_1/R = 0.25$ and L/D = 1, for Impact Mach Number of 0.2 and for Free-Slip Boundary Condition.

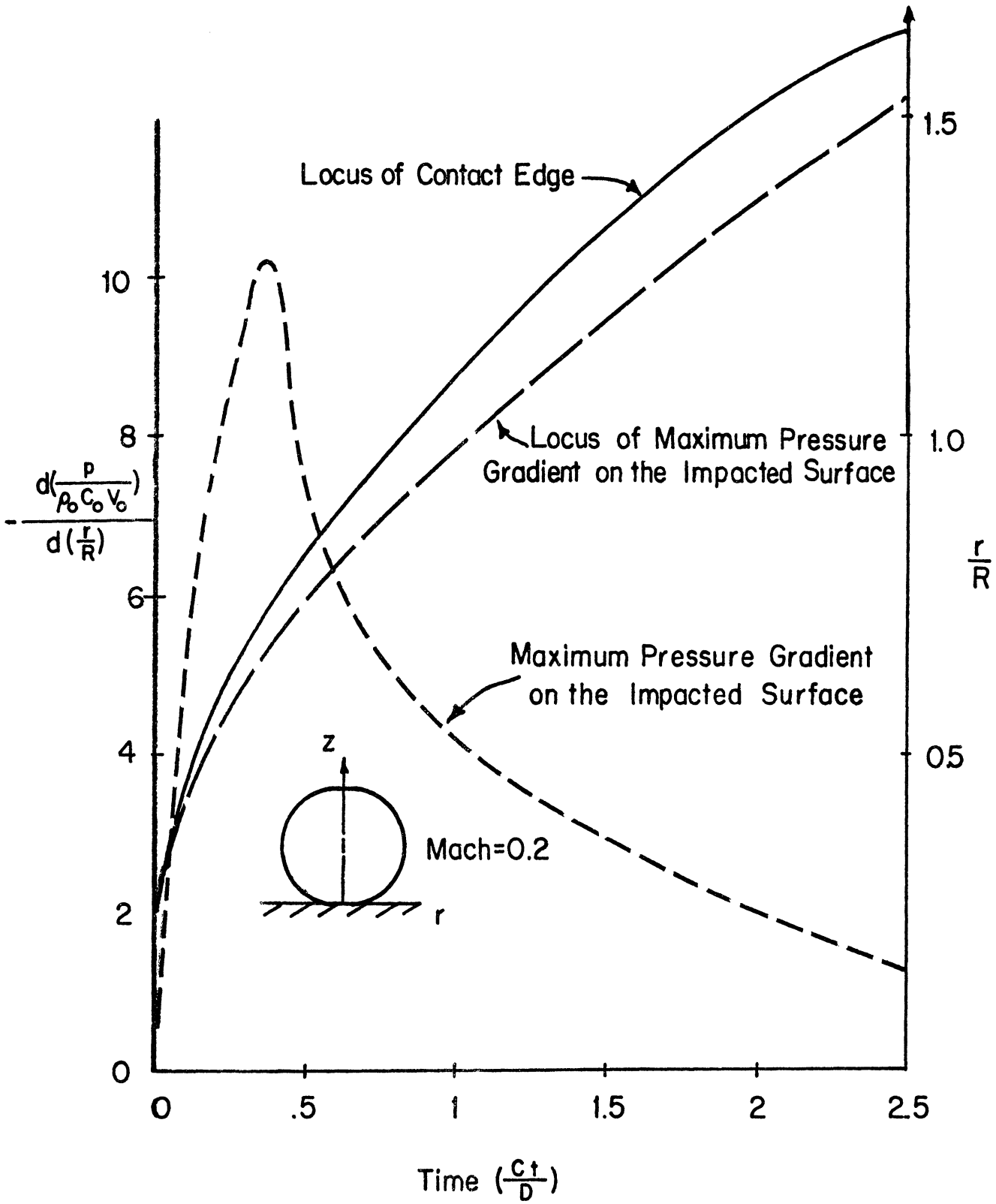

Fig. 7. Maximum Pressure Gradient-Time and -Location Relation and Contact Edge-Time History of an Initially Cylindrical-Spherical Composite Droplet with $R_1/R = 0.25$ and $L/D = 1$, for Impact Mach Number of 0.2 and for Free-Slip Boundary Condition.

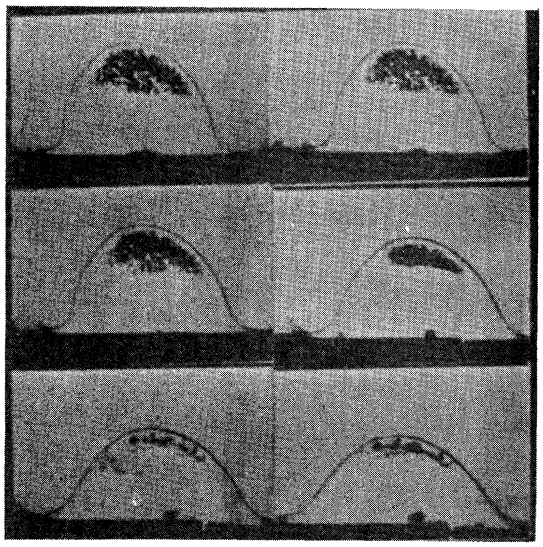

Fig. 8. Photographs of the Cavitation for a Water Droplet Following an Impact on a Solid Plane (Brunton and Camus[38])

IV. Concluding Remarks

The objective of this paper was to investigate the collision process between a rain drop and a rigid plane. Effort was directed to simulate this impact phenomenon. High-speed computation was employed to carry our the task. Results such as the deformation of the simulated rain drop, isobar distribution within the droplet at various instants, pressure distributions on the impact surface and everywhere within the computation domain were recorded by computer. Other variables such as density, velocity and momentum were also found as a function of time.

Since the liquid surface is free to deform, the pressure build-up is affected, from the first instant of impact, by the immediate radial release flow. Although an earlier more approximate analysis[39] postulates there is an initial stage during which no gross spreading or lateral outflow occurs, the present dynamic analysis finds that by the time incremented numerical approach used, the pressure gradient which exists at the contact edge will result in lateral flow immediately. For an impact Mach number of 0.2, which is equivalent to an impact velocity of 980 ft/sec. the maximum radial velocity is about 2750 ft/sec. These calculation results are in good agreement with the photographic observation in which radial velocity of 3056 ft/sec. resulted from an impact speed of 990 ft/sec., according to Fyall[21].

Negative pressure within the drop was computed, which could lead to actual cavitation, as a result of reflection of the pressure wave from the top surface of the droplet as a tension wave, as suggested earlier by Engel[19]. Very recent photographic evidence by Brunton and Camus[38] actually shows the fromation of such vapor pockets.

The maximum pressure in this simulated cylindrical-spherical rain drop is ~0.9 x the simple water hammer pressure $\rho_o C_o V_o$. The numerical results are thus between ~0.7 for spherical drop[37] and ~1.2 for cylindrical jet[34].

ACKNOWLEDGEMENT

The work was supported by National Science Foundation Grant No. GK 730.

REFERENCES

1. Honegger, E., "Tests on Erosion Caused by Jets," Brown Boveri Review, 14, 4, pp. 95-104, (1927).
2. Cook, S.S., "Erosion by Water-Hammer", Proc. Royal Society, A, 119, pp. 481-488, (1928).
3. Christie, D. G., and Hayward, G. W., "Observation of Events Leading to the Formation of Water Drops Which Cause Turbine Blade Erosion", Phil. Trans. Roy. Soc., A, Part No. 1110, 260, pp. 73-315, (1966).
4. Caldwell, J., "Description of the Damage in Steam Turbine Blading Due to Erosion by Water Droplets", Phil. Trans. Roy. Soc. A, Part No. 1110, 260, pp. 204-208, (1966).
5. Smith, A., "Physical Aspects of Blade Erosion by Wet Steam in Turbines", Phil. Trans. Roy. Soc., A, Part No. 1110, 260, pp. 209-215, (1966).
6. Schmitt, G. F. Jr., "Current Investigations in Rain Erosion by the U.S. Air Force," ASTM Meeting in Atlantic City, N.J., June 27-July 1, 1966.
7. Wahl, N.E., "Investigation of the Phenomena of Rain Erosion at Subsonic ans Sulersonic Speeds," Air Force Materials Laboratory Report AFML-TR-65-330, (1962).
8. Fyall, A.A., King, R.B., and Strain, R.N.C., "Rain Erosion Aspects of Aircraft and Guided Missiles", J. Roy, Aero. Soc., 66, pp. 447-453, (1962).
9. Naude, C.F., and Ellis, A.T., "On the Mechanism of Cavitation Damage by Nonhemispherical Cavities Collapsing in Contact with a Solid Boundary," Trans. ASME, J. Basic Engr., December, 1961.
10. Hammitt, F.G., "Observations on Cavitation Damage in a Flowing System", J. Basic Engr., Trans. ASME, 85, D, 3, pp. 347-359, (1963).
11. Knapp, R.T., Daily, J.W., and Hammitt, F.G., Caviatation, McGraw-Hill, (1970).
12. Pouchot, W.D., et al., "Analytical Investigation of Turbine Erosion Phenomena," Westinghouse Astro-Nuclear Lab. Report PR-(DD)-014, (1966).
13. Zimmerman, W.F., and Rossback, R.J., "Metallurgical and Fluid Dynamic Results of a 2000-hr. Endurance Test on a Two-Stage, 200-hoursepower Turbine in a Wet Potassium Vapor", ASME Paper 67-GT-9, (1967).

14. Wood, G.M., et al., "Cavitation Damage Investigation in Mixed Flow Liquid Metal Pumps", Symposium on Cavitation in Fluid Machinery, ASME, pp. 196-214, (1965).

15. Hammitt, F.G., "Two-Phase Material Attribution Problems for Rankine-Cycle Liquid Metal Power Plants," Trans. ASME, J. Engr. for Power, 88, A, 4, pp. 388-394, (1966).

16. Wengel, H.G., Jr., and Wang, C.T., "The Mechanics of a Drop After Striking a Stagnant Water Layer", Research Report No. 30, Water Resources Center, University of Illinois, (1970).

17. Worthington, A.M., A Study of Splashes, the MacMillan Company, New York, (1963).

18. Engel, O.G., "Mechanism of Rain Erosion", WADC Tech. Report 53-192, Part I through XV. (1953).

19. Engel, O.G., "Waterdrop Collisions with Solid Surfaces," J. of Research of the National Bureau of Standards, 54, 5 May 1955.

20. Bowden, F.P., and Brunton, J.H., "The Deformation of Solids by Liquid Impact at Supersonic Speeds", Proc. of the Royal Society, A, 263, pp. 433-450, (1969).

21. Fyall, A.A., "Single Impact Studies of Rain Erosion", Shell Aviation News, 374, (1969).

22. Tait, P.G., "Report on Some of the Physical Properties of Fresh Water and Sea Water", Report on Scientific Results of Voy, H.M.S., and Challenger, Phys. Chem., 2, 1-71 (1888).

23. Cole, R.H. Underwater Explosion, Dover (1965).

24. Li, Y-H. "Equation of State of Water and Sea Water" J of Geophysical Research, 32, 10, May 1967.

25. Heymann, F.J., "On the Shock Wave Velocity and Impact Pressure in High-Speed Liquid-Solid Impact," Trans. ASME, J. of Basic Engr., 90, p. 400, July 1968.

26. Kirkwood, J.G., and Bethe, H.A., "The Pressure Wave Produced by an Underwater Explosion; I, Basic Propagation Theory", 588, (1942).

27. Kirkwood, J.G., and Richardson, J.M., "The Pressure Wave Produced by an Underwater Explosion; III, Properties of Salt Water at a Shock Front," OSRD Report 813, (1942).

28. Richardson, J.M., et al., "Hydrodynamic Properties of Sea Water at the Front of a Shock Wave," J. of Chemical Physics, V. 15, II, pp. 785-794, (1947).

29. Rice, M.H., and Walsh, J.M., "Equation of State for Water to 250 kilobars," J. of Chemical Physics, 26, 4, pp. 825-830, April 1957.

30. Cook, M.A., et al., "Measurements of Detonation Pressure", J. Applied Physics, 33, 12., pp. 3413-3421, Dec. 1962.

31. Huang, Y.C., Hammitt,F. G. and Mitchell, T.M. "A Note on Shock Wave Velocity in High-Speed Liquid-Solid Impact", Report No. UMIC-033710-11-T, The University of Michigan, 1971.

32 Savic, P., and Boult, G.T., "The Fluid Flow Associated with the Impact of Liquid Drops with Solid Surfaces," National Research Council of Canada, Report No. MT-26, May 1955.

33. Heymann, F.J., "High-Speed Impact Between a Liquid Drop and a Solid Surface," J. of Applied Physics, 40, 13, pp. 5113-5122, Dec. 1969.

34. Huang, Y.C., Hammitt, F.G. and Yang, W.J., "Normal Impact of a Finite Cylindrical Jet on a Flat Rigid Plane," Report No. UMIC-033710-9-T, The University of Michigan, 1971.

35. Huang, Y.C., "Numerical Studies of Unsteady, Two-Dimensional Liquid Impact Phenomena," PhD Thesis, The University of Michigan, 1971.

36. Briggs, L.J., "Limiting Negative Pressure of Water", J. of Applied Physics, 21, July 1950, pp. 721-722.

37. Huang, Y.C., Hammitt, F.G. and Yang, W-T, "Impact of Spherical Water Drop on a Flat Rigid Plane," Report No. UMICH-033710-10-T, The University of Michigan, 1971.

38. Brunton, T.H., and Camus, T.T., "The Flow of a Liquid Drop During Impact," 3rd International Congress on Rain Erosion, August, 1970.

39. Bowden, F.P. and Field, T.F., "The Brittle Fracture of Solids by Liquid Impact, by Solid Impact, and by Shock," Proc. Roy Soc. (London) A282, 331, (1964).